Transverse modulus measurement of carbon fibre by atomice force microscope and nanoindentation

TRANSVERSE MODULUS MEASUREMENT OF CARBON FIBRE BY ATOMIC FORCE MICROSCOPE AND NANOINDENTATION

Shanghong Duan[1], Fang Liu[1], Torbjörn Pettersson[2], Claudia Creighton[3] and Leif Asp[1*]

[1] Industrial and Materials Science, Chalmers University of Technology, Gothenburg, Sweden
[2] Department of Fibre and Polymer Technology, KTH Royal Institute of Technology, Sweden
[3] Institute for Frontier Materials, Deakin University, Geelong, Australia.
* Corresponding author (leif.asp@chalmers.se)

Keywords: Transverse Young's modulus, Carbon fibre, FIB-SEM, AFM, Nano-indentation

ABSTRACT

Carbon fibre reinforced polymer composite has been widely used in structural component due to the high specific axial modulus of carbon fibre. However, the transverse Young's modulus is much lower and not well studied because of the extremely small diameter (~5 μm). In this work, flat test surfaces on carbon fibre IMS65 were fabricated using focused ion beam. The transverse Young's modulus was measured by nano-scale indentation tests, which were performed on fabricated flat surfaces, using both atomic force microscopy and nano-indentation. The surface damage induced by the high energy ion beam was also assessed.

1 INTRODUCTION

Carbon fibre, which has the highest specific modulus in axial direction, is one of the best materials for lightweight structure applications. Because carbon fibre is made of graphite crystals, it is also able to be used as anode material in lithium ion battery, where graphite is commercially used. Based on the multifunctionality of carbon fibre, structural battery is designed as an electrical energy storage multi-functional composite material [1]. However, the mechanical properties in transverse direction were less studied due to the extremely small diameter (~5 μm) of carbon fibre. Good knowledge of transverse mechanical properties of carbon fibre is beneficial for any application including structural battery, where carbon fibre acts as structural load carrier. It has been suggested that the transverse Young's modulus of carbon fibre may increase threefold after lithium intercalation [2]. Such increase in transverse modulus of carbon fibre would result in up to 43% increase of the transverse Young's modulus of whole structural battery composite [3]. Therefore, in order to accurately model the mechanical properties and the internal stresses of structure battery, an accurate and reliable method to measure the transverse Young's modulus of carbon fibre is required for future study.

In present work, the transverse Young's modulus of carbon fibre IMS65 was measured by nano-scale indentation tests in transverse direction using atomic force microscopy (AFM) and nano-indentation. Flat surfaces on carbon fibre were fabricated and cleaned using focused ion beam (FIB). The surface damage induced during milling process was also studied and discussed. In the future, the established experimental method will be employed to measure both pristine and lithiated carbon fibres.

2 EXPERIMENT AND ANALYSIS METHODS

2.1 Sample preparation

Flat surface on carbon fibre was fabricated using focused ion beam as shown in Fig. 1. In this work, Versa 3D produced by FEI company was employed. A single IMS65 carbon fibre was picked and glued onto a silicon wafer with silver paint. The specimen was then transported into the FIB-SEM and coated with beam ion assisted Pt deposition in a 5×25 μm area on both sides of carbon fibre at the milling position. The Pt coating is needed to protect the surface in the milling process and to fix the test part during the following indentation tests. In FIB-SEM, accelerated Ga^+ ions shoot on the carbon fibre in a direction parallel to the silicon wafer substrate and knock out carbon atoms. One should be

aware that FIB milling generally induces amorphous surface damage and Ga implant, which has been observed in silicon using transmission electron microscopy (TEM) [4]. To thin down the amorphous surface damage, milled surfaces were then sputtered by 5 keV Ga^+ ion beam with current 77 pA and incident angel of 7° in 3 mins. The milling process is described in detailed in Fang's work [5].

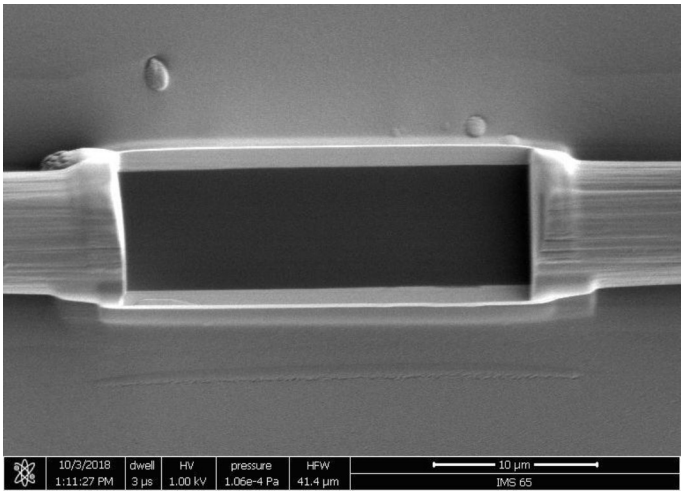

Figure 1: Flat surface milled by FIB.

2.2 Indentation test

Indentation tests have been widely used to determine mechanical properties, such as elastic modulus and hardness [6]. In this work, both AFM and nano-indentation are employed to preform indentation tests on the FIB milled flat surface on carbon fibres.

The indentation test in AFM was performed using MultiMode III with Picoforce extension (Veeco Instruments, Santa Barbara, CA, USA). Diamond tips (NM-TC, Brucker) was selected with tip radius around 30 nm. The tip was placed in the center of the flat surface. The ramp distance was set to 1 µm with ramp rate 200 nm/s. Each surface was measured by 20 indentations at different positions. Both sapphire and HOPG thin films (Brucker) were measured as reference materials. A schematic diagram of AFM is shown in Fig. 2 (left). During the test the deflection voltage ΔV and piezo displacement δ are recorded. The force F and indentation displacement δ were calculated using software AFM ForceIT v3 (ForceIT, Sweden) with following Equations:

$$F = k \times \sigma \times \Delta V \quad (1)$$

$$\delta = d - \sigma \times \Delta V \quad (2)$$

where k is spring constant, d is the displacement of sample holder and σ is detector sensitivity, which need to be calibrated by using reference materials.

The nano-indentation tests were performed using Bruker's Hysitron TI 980 TriboIndenter with test force 1000 µN, which results in 80-100 nm indentation depth. The tip shape is accuralty measured with SPM (Scanning probe microscopy). Polycarbonate (PC) sample was used as reference material. The indentation tests were performed in a raster over on FIB milled surface with a step size 400 nm. A schematic diagram of nano-indentation is shown in Fig. 2 (right).

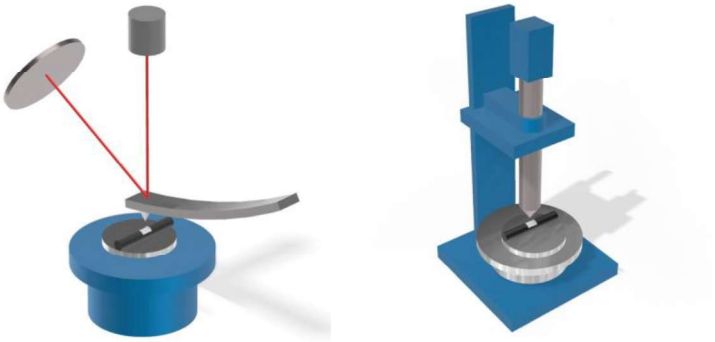

Figure 2: Schematic diagram of AFM (left) and nanoindentation (right) instruments.

To evaluate the cleanning process and remaining surface damage, indentation tests were perfomed also on a sample without the final cleaning step. The indentation results on cleaned and non-cleaned surface from AFM were compared to prove the existence of the amorphous layer. Indentation tests on cleaned surface were performed using both AFM and nano-indentation. Because the indentation depth in two instruments are different, the indentation results from AFM and nanoindentation can be used to compared to estimate the effectivity of the cleaning step.

2.3 Analysis models

From each indentation test, a loading and unloading curve is captured. A typical indentation load-displacement curve is shown in Fig. 3. Both Hertz model and Olive & Pharr model were used to analyze the indentation curves in this work. The main difference between the two methods is the data to be used. Hertz model use the elastic loading part, while Oliver & Pharr only considers the initial unloading part.

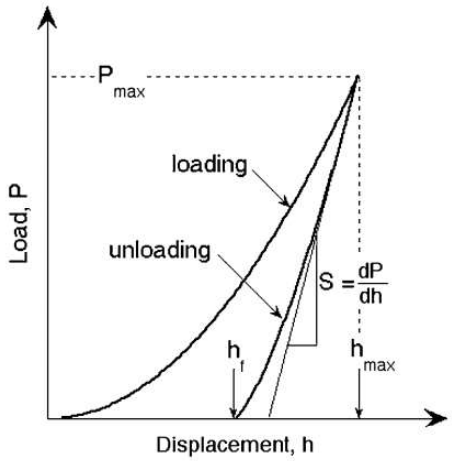

Figure 3: Schematic illustration of indentation force-displacement curve [7]. The initial elastic loading part can be analyzed with the Hertz model, while the Oliver & Pharr model can be used in the initial unloading part.

Hertz model

Hertz model describes pure elastic contact behaviour between an indenter probe and an infinite half space. In this work, it was selected to analyze the data from AFM tests due to the extremely low indentation depth (~5 nm), where pure elastic deformation is expected. As proof for pure elastic behaviour is the unloading curve exactly overlap the loading curve in AFM tests. From an indentation

force-displacement curve, the effective Young's modulus is extracted by fitting the curve according to following equation,

$$F = \frac{4}{3} E^* \sqrt{R\delta^3} \tag{3}$$

where the F is the load force, R is the tip radius, δ is the indentation displacement and E^* is the effective Young's modulus of specimen. The tip radius needs to be calibrated by the reference material. In this work, Eq. 3 was further transformed into linear relationship by power 2/3 on both sides as

$$F^{\frac{2}{3}} = \left(\frac{4\sqrt{R}}{3} E^*\right)^{\frac{2}{3}} \delta \tag{4}$$

E^* can be calculated from the slop of $F^{2/3}$-δ curves [8]. The real Young's modulus can be transferred from E^* through the following relationship,

$$\frac{1}{E^*} = \frac{1 - {v_i}^2}{E_i} - \frac{1 - v^2}{E} \tag{5}$$

where v_i and E_i are the Poison ratio and Young's modulus of indenter, and v and E are the Poison ratio and Young's modulus of the sample. An additional benefit from Hertz model is that it can be modified to analyze orthotropic material with routine suggested by Swanson [9], which has been proved working successfully in our following work.

Oliver and Pharr model

The force-displacement curves from nano-indentation were analyzed by Oliver & Pharr model [7] due to a much deeper indentation depth (~100nm) where the loading curves are considered to be elastic-plastic. Considering the much deeper indentation depth and cleaning process during specimen fabrication, influence of the surface damage layer is assumed to be neglectable. The unloading curve is fitted by a power-law equation suggested by Oliver & Pharr,

$$P = \alpha\left(h - h_f\right)^m \tag{6}$$

where α and m are fitting parameters, h_f is the end indentation depth of unloading curve. The contact stiffness S is defined as the slop of the initial unloading curve as shown in Fig. 3:

$$S = \frac{dP}{dh} \tag{7}$$

Furthermore, the effective Young's modulus E^* can be calculated from the contact stiffness S as

$$E^* = \frac{S\sqrt{\pi}}{2\beta\sqrt{A_C}} \tag{8}$$

where β is geometry factor of the indenter and A_c is the contact area, which can be obtained by SPM. Once the effective Young's modulus is known, the Young's modulus of sample can be calculated with Eq. 5.

3 RESULTS

3.1 Indentation test from AFM

Indentation tests on both non-cleaned and cleaned surface were performed in AFM. Twenty curves were captured for each sample. The indentation depth under 1800 nN is around 5 nm. The tip radius is calibrated as 52.70 nm. Due to the thermal drift, approximate 1 nm shaking of the displacement can not be avoided, which causes scattering results as shown in Tab. 1. However, the force-displacement plots still show a good consistence between all indentation tests as shown in Fig. 4 (a). The influence

from thermal drift can be minimized by increasing the number of groups of data because it is statically random and can balance each other. The average effective Young's modulus E^* from 20 tests on non-cleaned surface is 13.39±2.34 GPa. With an assumption of Poisson's ratio as 0.28, the transverse Young's E_T is calculated as 14.53±2.51 GPa using Eq. 5.

Test Nr.	Effective Young's modulus E^* /GPa	Test Nr.	Effective Young's modulus E^* /GPa	Test Nr.	Effective Young's modulus E^* /GPa
1	11.34	8	15.45	15	16.40
2	14.11	9	10.71	16	10.36
3	15.47	10	11.56	17	10.22
4	15.03	11	13.25	18	14.96
5	11.24	12	10.61	19	14.70
6	18.00	13	10.98	20	15.36
7	14.88	14	13.20		

Table 1: Effective Young's modulus of IMS65 non-cleaned sample in AFM

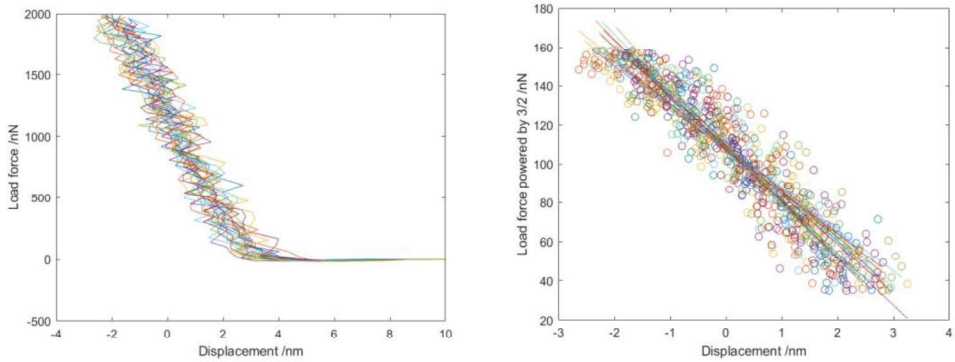

Figure 4: a) Indentation curves on IMS65 non-cleaned surface from AFM tests, b) linear fitting of indentation curves in $F^{2/3}$-δ plots (fitting force range from 200 to 2000 nN).

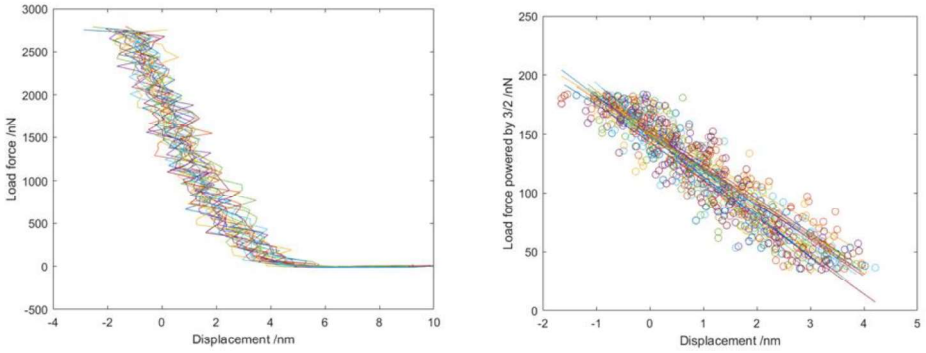

Figure 5: a) Indentation curves on IMS65 cleaned surface from AFM tests, b) linear fitting of indentation curves in $F^{2/3}$-δ plots (fitting force range from 200 to 2000 nN).

The indentation curves from cleaned surface are shown in Fig. 5 and the effective Young's modulus E^* were extracted with calibrated tip radius 30.09 nm as listed in Tab. 2. The average E^* on cleaned surface turns to be 24.26±4.24 GPa, which is corresponding to a E_T of 26.32±4.61 GPa. This result is much higher than that from indentation tests on non-cleaned surface. The only difference between two experiments is the low energy Ga^+ cleaning process. The higher result from cleaned

surface indicates an existence of a softer amorphous damage layer on non-cleaned surface and prove the cleaning process can thin down this damage layer.

Test Nr.	Effective Young's modulus E^* /GPa	Test Nr.	Effective Young's modulus E^* /GPa	Test Nr.	Effective Young's modulus E^* /GPa
1	26.89	8	31.96	15	20.96
2	26.15	9	22.02	16	20.97
3	23.47	10	22.60	17	33.22
4	19.75	11	29.32	18	25.82
5	17.91	12	20.65	19	25.74
6	29.27	13	24.04	20	19.48
7	21.09	14	23.90		

Table 2: Effective Young's modulus of IMS65 cleaned sample in AFM.

3.2 Indentation test from nano-indentation

Comparing with the indentation test in AFM, nano-indentation tests were performed at a much larger indentation depth (80-100 nm). The influence from the thermal drift and amorphous damage layer can be neglected in these tests. A map with effective Young's modulus E^* of fibre IMS65 is shown in Fig. 6. The homogeneity is shown by the consistent results over the surface. E^* increases at the edge of the carbon fibre, where the milled surface cannot be considered as infinite half space anymore due to the presence of Pt coating. Furthermore, due to the circular cross section shape, the thickness of the carbon fibre close to the edge is also not enough to fulfill one of the assumptions in Oliver & Pharr model, which requires the thickness of the half space should be at least 10 times higher than the indentation depth. The effective Young's modulus E^* results in the middle area (marked in a red frame in Fig. 6) are collected as valid resource, which gives an average E^* equal to 24.63±0.67 GPa and E_T equal to 26.73±0.72 GPa. Those results are consistent with the AFM tests on cleaned surface, where only 0.37 GPa and 0.41 GPa difference are found in E^* and E_T, respectively. The consistence between AFM and nanoindentation results on cleaned surface indicates that the cleaning step decrease the thickness of the amorphous layer, which eliminates the influence from the softer amorphous layer on the indentation results.

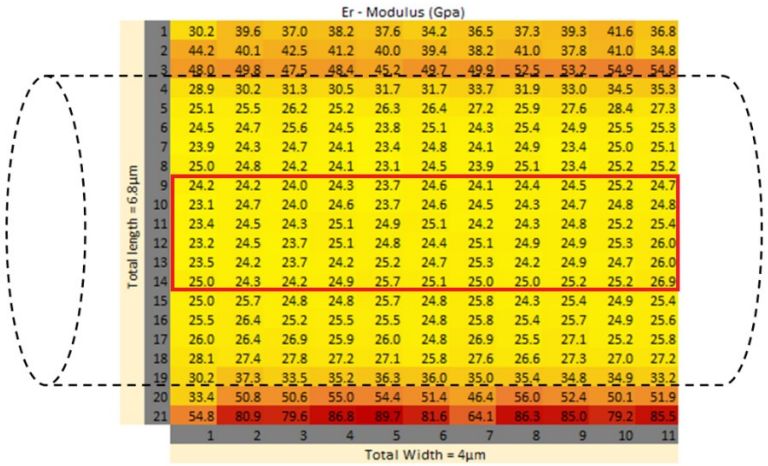

Figure 6: Effective modulus E^* from Nano-indentation tests (results in the red frame are considered as valid results).

4 CONCLUSIONS

In this work, the transverse Young's modulus ET of carbon fibre IMS65 was measured by both AFM and nano-indentation. It is proven that the high-energy ions milling process can damage the turbostratic graphitic structure and cause the formation of amorphous surface layer which is softer than the non-damaged crystal structure. However, a cleaning step with low energy Ga+ ions eliminates most of the amorphous layer. Both AFM and nanoindentation provide very consistent result on cleaned specimen despite different indentation depths and different analysis models. The extracted ET is 26.32±4.61 GPa and 26.73±0.72 GPa from AFM and nanoindentation, respectively.

ACKNOWLEDGEMENTS

This work was funded by USAF office of scientific research (Award no.: FA9550-17-1-0338), and EU Horizon 2020 under Grant Agreement Number 738085. FL and LA acknowledge support from LIGHTer, a program financed within Strategic Innovation Areas, a mutual venture between VINNOVA, the Swedish Energy Agency, and Formas. FL also acknowledges funding from the Swedish Energy Agency (project nr. 46598-1).

REFERENCES

[1] L.E. Asp and E.S. Greenhalgh, Structural power composites, *Composite Science and Technology*, Vol. 101, pp 41-61, 2014.

[2] Y. Qi, H. Guo, L.G. Hector and A. Timmons, Threefold increase in the Young's modulus of graphite negative electrode during lithium intercalation, *J. Electrochem. Soc.*, **157(5)**, 2010, pp. A558-66.

[3] D. Carlstedt, E. Marklund and L.E. Asp, Effects of state of charge on elastic properties of 3D structural battery, *Composite Science and Technology*, **169**, 2019, pp. 26-33.

[4] L A. Giannuzzi, R. Geurts and J Ringnalda, 2 keV Ga+ FIB Milling for Reducing Amorphours Damage in Silicon, *Micro Microanal*, **11**, 2005, pp. 828-829.

[5] F. Liu, S. Duan and L. Asp, Specimen preparation for transverse modulus measurement of carbon fibres using focused ion beam, *Proceedings of the 22^{dth} International Conference on Composite Materials, August 11-16, 2019.*

[6] A.C. Fischer-Cripps, A review of analysis methods for sub-micron indentation testing, *Vacuum*, **58**, 2000, pp. 569-585.

[7] W.C. Oliver and G.M. Pharr, An improved Technique for Determining Hardness and Elastic Modulus Using Load and Displacement Sensing Indentation, *J. Mater. Res.*, **7**, 1992, pp. 1564-83.

[8] P. Carl and H. Schiller, Elastic measurement of living cell with an atomic force microscope: data acquisition and processing, *Pfluger Arch-Eur J physiol*, **457**, 2008, pp. 551-559.

[9] S.R. Swanson, Hertzian contact of orthotropic materials, *International Journal of Solids and Structures*, **21**, 2004, pp. 1945-59.